Experimental method to account for structural compliance in nanoindentation measurements

J.E. Jakes[a)]
Materials Science Program, University of Wisconsin—Madison, Madison, Wisconsin 53706; and United States Department of Agriculture (USDA) Forest Products Laboratory, Madison, Wisconsin 53726

C.R. Frihart, J.F. Beecher, and R.J. Moon
United States Department of Agriculture (USDA) Forest Products Laboratory, Madison, Wisconsin 53726

D.S. Stone
Materials Science Program, University of Wisconsin—Madison, Madison, Wisconsin 53706; and Department of Materials Science and Engineering, University of Wisconsin—Madison, Madison, Wisconsin 53706

(Received 10 October 2007; accepted 10 January 2008)

The standard Oliver–Pharr nanoindentation analysis tacitly assumes that the specimen is structurally rigid and that it is both semi-infinite and homogeneous. Many specimens violate these assumptions. We show that when the specimen flexes or possesses heterogeneities, such as free edges or interfaces between regions of different properties, artifacts arise in the standard analysis that affect the measurement of hardness and modulus. The origin of these artifacts is a structural compliance (C_s), which adds to the machine compliance (C_m), but unlike the latter, C_s can vary as a function of position within the specimen. We have developed an experimental approach to isolate and remove C_s. The utility of the method is demonstrated using specimens including (i) a silicon beam, which flexes because it is supported only at the ends, (ii) sites near the free edge of a fused silica calibration standard, (iii) the tracheid walls in unembedded loblolly pine (Pinus taeda), and (iv) the polypropylene matrix in a polypropylene–wood composite.

I. INTRODUCTION

When Oliver and Pharr[1] originally derived what has now become the most commonly applied method for analysis of nanoindentation data, they constructed it based on a study of bulk, homogeneous materials. This "standard" method implicitly relies on the assumptions that the specimen be homogeneous, that it fill a half-space, and that it be rigidly supported in the testing machine. Notably, though, the greatest potential of nanoindentation is reached when it is used to study specimens that violate these assumptions: specimens that are themselves extremely small, or specimens that possess heterogeneities with length scales comparable to the nanoindents themselves.

Our interest in the applicability of nanoindentation stems from our investigations of the mechanical properties of wood. In recent years, scientists have used nanoindentation to study tracheid walls in softwood trees[2–6] and to investigate the effects of chemical additions[7–9] and heat treatments[10] on the mechanical properties of the walls. The tracheid is the predominant type of cell found in softwood, and a transverse cross section of a tracheid is illustrated in Fig. 1. A tracheid is basically a hollow cylindrical tube with a wall composed of several concentric laminations. Individual tracheids are held together by the middle lamella. Although the standard nanoindentation analyses have proven to be a useful tool for wood science research, the nonuniform structure of the tracheid walls violates the fundamental mechanics assumptions underlying these analyses. For instance, whereas a typical nanoindent might be 1 μm in diameter and positioned in the thickest layer of the tracheid wall (labeled S2 in Fig. 1), the layer itself is typically only 3 to 7 μm wide in latewood cells. This means that indents in this layer are always close to the other tracheid wall layers (S1, S3, and primary), lumen, and middle lamella. Even though the indent may never touch these other features, the features nevertheless give rise to mechanical discontinuities that alter the deformation fields surrounding indents. Because of their thinness, tracheid walls also have the potential to flex and buckle during nanoindentation, processes that are unaccounted for in the Oliver–Pharr analysis.

We have developed tools to help apply nanoindentation to wood and other nonideal systems. Our interests lie

[a)]Address all correspondence to this author.
e-mail: jjakes@fs.fed.us
DOI: 10.1557/JMR.2008.0131

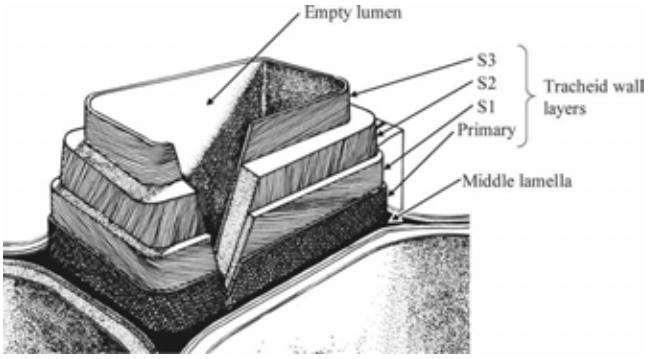

FIG. 1. Typical tracheid in softwood.

in two types of departure from the ideal system assumed in the standard analyses [Figs. 2(a) and 2(b)]. The first departure comes from specimens that flex under loading. Figure 2(a) depicts the specimen as an annulus or hollow tube such as a mouse bone[11]; but in principle the flexible specimen can be of any shape or held under any support that allows for large-scale elastic displacements. The second departure is the edge problem, which is inherent to specimens that possess a high degree of heterogeneity at length scales comparable to the size of the nanoindents. In this case, nanoindents located near a free edge or interface between phases perpendicular to the indented surface [Fig. 2(b)] are affected. We shall demonstrate experimentally that the departures represented by Figs. 2(a) and 2(b) give rise to systematic errors in the standard Oliver–Pharr analysis because they produce an additional compliance term that must be accounted for in the analysis. We call this compliance the structural compliance

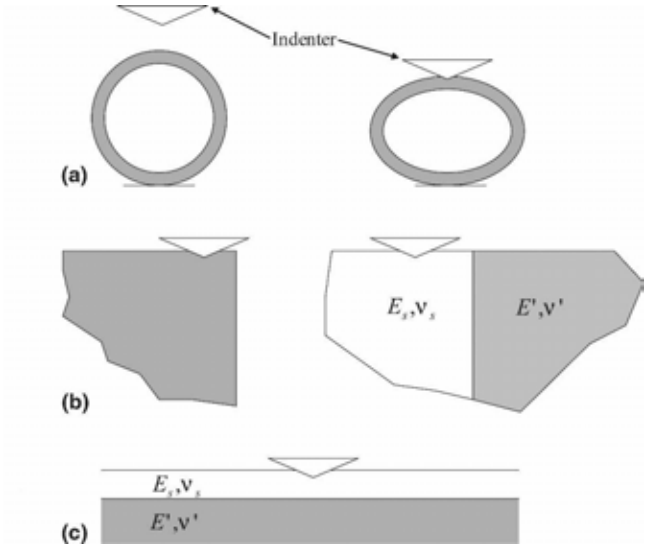

FIG. 2. Sources of structural compliance. (a) Specimen-scale deformation. (b) Elastic heterogeneities such as a free edge or interface with a dissimilar material. (c) Layered specimen. This paper primarily addresses situations (a) and (b).

(C_s), and an analysis technique to calculate and account for C_s is presented in this paper. A third departure comes from nanoindentation of a material with an interface parallel to the surface, such as a thin film on a substrate [Fig. 2(c)]. This problem has already been treated both theoretically and experimentally,[12–15] but is included here for completeness. In the discussion we examine similarities between the thin-film–substrate configuration and the other two geometries.

The need for a nanoindentation method capable of separating the intrinsic properties of a material from the effects of a nearby free edge or elastic discontinuity has been identified numerous times. For instance, Choi et al.[16] and Soifer et al.[17] investigated patterned aluminum and copper lines, respectively, and Ge et al.[18] investigated flat-topped wedges etched in silicon. In these studies no attempts were made to quantify material properties near the edge. The authors all noted that the nanoindentation analyses available were not applicable near the edge. Hodzic et al.[19] probed the interphase regions of polymer–glass composites and found that hardness and elastic modulus values rose dramatically as indents in the polymer matrix were placed close to the fibers. They concluded that these increases could not result solely from changes in properties in the interphase region and must be influenced by the close proximity of the higher-modulus and higher-hardness glass fiber. Downing et al.[20] also performed nanoindentation experiments on polymer–glass composites and found that the apparent elastic modulus of the matrix increased as the indents approached the fiber. However, when the fiber was removed by chemical etching and the same nanoindentation experiments were performed, the apparent elastic modulus decreased as the vacant hole was approached. Lee et al.[21] recently evaluated the interphase properties of a cellulose fiber-reinforced polypropylene composite by nanoindentation and finite element analysis. From the nanoindentation measurements, they reported increases in the properties of the matrix as the cellulose fiber was approached. However, from the finite element analysis, they observed that the same increase in measured properties would be caused by the close proximity of the interface between the polypropylene and cellulose fiber. They concluded the material properties of the matrix could not be separated from the effects of the nearby fiber using existing nanoindentation techniques. Below, we show how to perform this separation.

II. BACKGROUND

A. Standard Oliver–Pharr analysis

In the Oliver–Pharr method,[1] the area of a nanoindent is determined based on depth and calibrated indenter shape. From a nanoindentation load–depth (L)–(h) trace

that has been corrected for machine compliance, the Meyer's hardness (H) may be calculated from

$$H = \frac{L_{\max}}{A} \quad , \tag{1}$$

where $L_{\max}$ is the load immediately prior to unloading and A is the projected indent area at $L_{\max}$. In turn, in the standard analysis A is estimated based on contact depth, h_c, defined as

$$h_c = h_{\max} - \epsilon L_{\max} C_p \quad , \tag{2}$$

where $h_{\max}$ is the maximum depth, C_p the unloading compliance attributable to the specimen and indenter, and ϵ is a geometric constant approximately equal to 0.75 for a Berkovich indenter. C_p can be related to specimen and indenter properties using

$$C_p = \frac{1}{E_{\text{eff}} A^{1/2}} \quad , \tag{3}$$

where E_{eff} is an "effective" modulus for contact given by

$$\frac{1}{E_{\text{eff}}} = \frac{1}{\beta}\left(\frac{1-\nu_s^2}{E_s} + \frac{1-\nu_d^2}{E_d}\right) \quad , \tag{4}$$

where E_s and E_d are Young's moduli and ν_s and ν_d are Poisson's ratios of specimen and indenter, respectively. β is a numerical factor, which is usually assumed to be $2/\pi^{1/2} = 1.128$. Recent authors[22–24] have reported that the conventional value is too low and that the actual value, which varies a little depending on specimen properties and indenter shape, is closer to 1.2. At present, we find that $\beta \cong 1.23$ works best based on our analysis of indents placed in a fused silica standard. We will therefore use $\beta \cong 1.23$ in both the standard analysis and our "corrected" analysis throughout what follows.

B. Corrected analysis accounting for structural compliances

Beginning with a load–depth trace that is not corrected for the machine compliance (C_m), the total measured unloading compliance (C_t) obtained from a semi-infinite, homogeneous specimen is given by

$$C_t = C_p + C_m \quad . \tag{5}$$

However, based on our own experimental evidence, we shall assert that in addition to the usual C_m in Eq. (5), other sources of compliance are present when the experiment is performed on specimens such as those in Figs. 2(a) and 2(b), and that these compliances introduce artifacts into the standard determination of E_s and H. These added "structural" compliances (C_s) may arise, for instance, from the presence of nearby free edges or other elastic discontinuities, from the finite size of the specimen, from the flexing of the specimen because of the way it is mounted, or, in the case of cellular structures such as wood, the bending and buckling of cell walls. These added compliances behave much the same way that C_m does because they contribute additively to the measured compliance and because, to close approximation, they are independent of the size of the indent. Therefore, to accurately determine C_p from Eq. (5), an additional term, C_s, must be added to the right-hand side. However, unlike C_m, which is a consistent property of the machine, C_s can be highly sensitive to position within a given specimen. Taking this assertion into account, Eq. (5) may be rewritten as

$$C_t = \frac{1}{E_{\text{eff}} A^{1/2}} + (C_m + C_s) \quad , \tag{6}$$

where we have substituted for C_p from Eq. (3) and included the additional term C_s. Following a method first proposed by Doerner and Nix[25] to isolate machine compliance, $C_m + C_s$ in Eq. (6) can be determined as the intercept in a plot of C_t as a function of $A^{-1/2}$ for a series of indents over a range of loads, in which case the data form a straight line whose slope is $1/E_{\text{eff}}$. This kind of plot will be called a "DN plot." Obviously, the analysis works only if $C_m + C_s$ and E_{eff} remain constant over the series of indents. To construct an accurate DN plot in the presence of a large and unknown structural compliance, the areas of the indents must be measured directly, instead of relying on the assumed area based on h_c, because accurately calculating A in Eq. (6) is impossible if C_s is unknown.

Another useful correlation that can also be easily modified from its original form to include the effects of C_s was discovered by Stone, Yoder, and Sproul (SYS).[14] If the square root of load is multiplied by the unloading compliance, then Eqs. (1) and (6) can be used to derive

$$C_t L_{\max}^{1/2} = (C_m + C_s) L_{\max}^{1/2} + J_0^{1/2} \quad , \tag{7}$$

where $J_0 = H/E_{\text{eff}}^2$ is the Joslin–Oliver[26] parameter. According to Eq. (7), provided that there is no indentation size effect in the properties (i.e., J_0 a constant), $C_t L_{\max}^{1/2}$ plotted as a function of $L_{\max}^{1/2}$ forms a straight line of slope $C_m + C_s$. The properties of the specimen are represented exclusively by the intercept. In what follows, we refer to data presented in the form of Eq. (7) as a "SYS plot."

In experiments where the value of C_s could change with indent location, it is advisable to determine C_s independently at each indent location. Fortunately, the data necessary to construct a SYS plot can be obtained from a single indent location by determining the contact stiffness as a function of load using either multiload indents or dynamic stiffness measurements.[23] The SYS plot works best when there is no indentation size effect in the properties, but even when there is an indentation size

TABLE I. Specimens indented in this study.

Specimen	Source of structural compliance
(100) silicon wafer	Specimen flexing
Fused silica	Edge effects
Loblolly pine (Pineas taeda)	Edge effects; cellular structure
Polypropylene–wood composite	Elastic heterogeneity

effect the SYS plot or a variation of it can be very useful for analyzing data.

III. EXPERIMENTAL WORK

In this work we investigate two broad classes of structural compliance, namely the large-scale bending or flexing of the specimen [Fig. 2(a)] and the presence of elastic heterogeneities, such as a nearby free edge or stiff reinforcement phase [Fig. 2(b)]. In most cases the added compliance is positive, but when the source of compliance is a nearby phase whose Young's modulus is greater than that of the phase being tested, the stiffening effect caused by the nearby phase gives rise to a negative structural compliance. To elucidate these systematic effects, experiments are performed on the four different systems shown in Table I. In all cases involving free edges or structural heterogeneities, it is presumed that all features intersect the surface at right angles. An alternative situation is where the specimen is layered [Fig. 2(c)] with the layers parallel to the surface. In this case, it is not possible to treat the substrate as giving rise to a structural compliance, independent of the size of the indent, unless the indent is made smaller than the thickness of the surface layer.[13]

A. Specimens

A beam cut from 0.5-mm-thick (100)-oriented silicon (Polishing Corporation of America, Santa Clara, CA) was studied to investigate the effects of compliant support. A fused silica standard (Hysitron, Minneapolis, MN) was studied to investigate the effects of a nearby free edge. These specimens were tested in the as-received condition. Specimens of wood and wood–polypropylene composite were also studied. These specimens required special preparation.

To investigate structural compliance in wood, specimens from the transverse cross sections in the latewood of plantation-grown loblolly pine (Pinus taeda) were prepared for nanoindentation experiments. Previous researchers have either embedded their wood specimens in an epoxy[2,4,5,7–9,27] or ground and polished the specimens.[10] However, to limit the amount of mechanical damage on the surface and eliminate the possibility of any undesired chemical modifications caused by the epoxy, a surface preparation procedure was developed to eliminate these possible artifacts. First, a 10-mm cube of loblolly pine was selected with no visible defects. A gently sloping (~15°) apex was created using a microtome on the transverse surface of the cube with the apex positioned in the latewood band (Fig. 3). Next, a sledge microtome fit with a custom-built diamond knife holder was used to cut the tip of the apex. The result was an exceptionally smooth and flat surface area of approximately 0.5 mm^2. Best results were achieved when the clearance and cutting angles were set to approximately 5°. We believe that this surface preparation technique allows the measurement of in situ mechanical properties of the tracheid walls with fewer artifacts than achieved with other surface preparation techniques.

A polypropylene–wood composite composed of a polypropylene matrix and wood flour was also studied. The formulation of the composite was 58.9 wt% wood flour, 33.8 wt% polypropylene, 4.0 wt% talc, 2.3% AC950P (maleated copolymer) (Honeywell, Morristown, NJ), and 1.0 wt% Optipak-100 (Honeywell). The morphology of the composite consisted of isolated wood tracheids, small clusters of tracheids, and small particles of talc or other wood debris dispersed within the

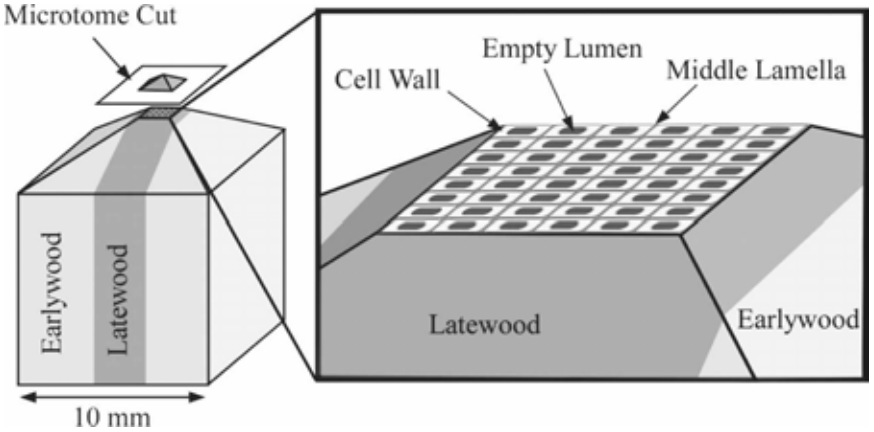

FIG. 3. Sample preparation of unembedded loblolly pine specimens.

polypropylene matrix. Further details about the formulation and manufacturing process are provided by Slaughter.[28] The procedure for preparing the polypropylene–wood composite specimen for nanoindentation was similar to that for the unembedded wood specimen described previously. First, a 10-mm cube was cut from the composite, with the surface to be tested oriented perpendicular to the extrusion direction. On this surface a gently sloping (~15°) apex was microtomed. After cooling with liquid nitrogen, the specimen was placed in the sledge microtome, and in one cut the tip of the apex was sliced off with a diamond knife, revealing a surface suitable for nanoindentation experiments. Again, the clearance angle and cutting angle were set to approximately 5°.

B. Nanoindentation procedure

A Hysitron Triboindenter equipped with a diamond Berkovich tip was used in this study. Standard methods were used to calculate the machine compliance and area function (based on contact stiffness) using a series of indents in the center of the fused silica standard with loads ranging from 0.05 to 10.00 mN. As previously mentioned, the area function was calculated using $\beta = 1.23$, not $\beta = 1.128$, which is commonly used in the literature. Based on this series of indents, the machine compliance was determined to be 2.7 ± 0.1 μm/N for the indenter configuration used in this study (uncertainty determined by least squares analysis of linear fit).

The experiments in this study used multiload indents in force control. The multiload indent load function consisted of 1 s loading segments, 15 s holds at partial loads, 5 s unloading segments, and 5 s holds at the partial unloads. There were seven loading segments that loaded to loads of 5%, 12%, 22.5%, 35%, 50%, 70%, and 100% of the final maximum load. Each partial unload was to 25% of the previous partial load, and the final partial unload was held for 60 s to calculate thermal drift before complete unloading.

Typical load–depth data from fused silica and wood are shown in Figs. 4(a) and 4(b), respectively. In fused silica [Fig. 4(a)], the data contain no appreciable viscoelastic rebound, as demonstrated by the lack of jog in the load–depth data from the 60 s hold and the minimal unloading–reloading hysteresis. Data from silicon (not shown) show behavior similar to that of fused silica. In contrast, the wood data [Fig. 4(b)] contain a viscoelastic rebound, which causes hysteresis loops to appear in the unloading–reloading data, and the jog in the final unloading slope from the 60 s hold. The viscoelastic rebound dies away after 10 to 15 s, and when calculating the thermal drift from the 60 s-hold period, the first 15 s must be omitted. A small amount of adhesion between the tip and tracheid wall is evident from the dip below zero load during the final unloading. The load–depth data from

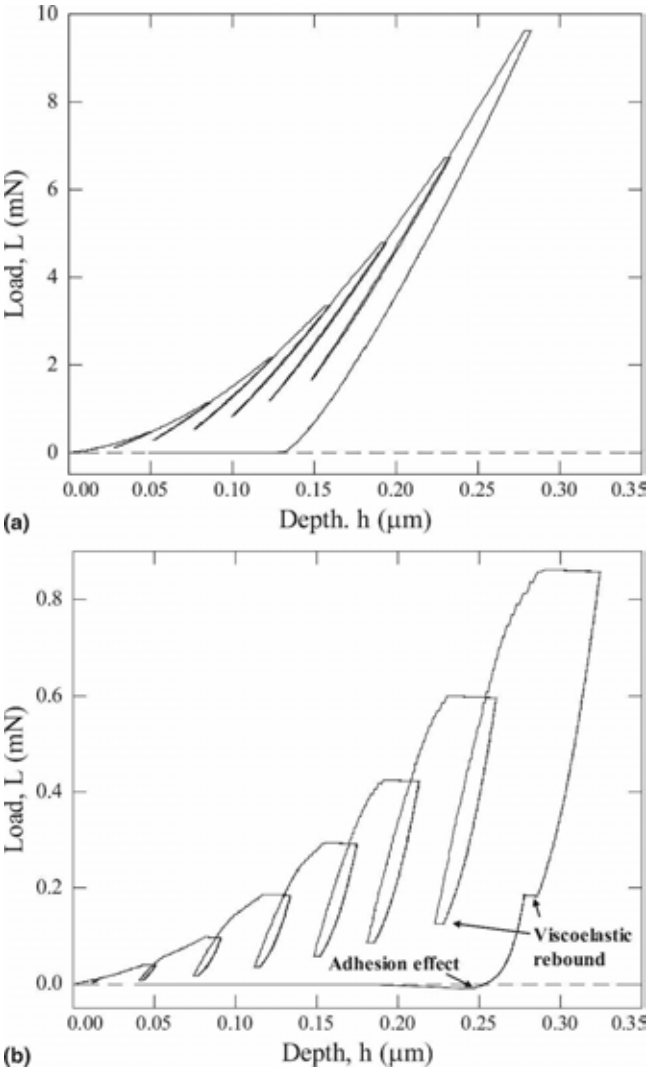

FIG. 4. Typical load–displacement curve (drift subtracted) for multiload indents performed in (a) fused silica and (b) S2 layer of a tracheid wall. The standard analysis was performed using data from the hold at maximum load and final unloading segment.

polypropylene (not shown) show behavior similar to that of wood, with noticeable viscoelastic rebound and adhesion during final unloading.

Young's moduli (E_s) of the materials in this study were calculated using Eq. (4), where E_d and ν_d for the diamond tip were assumed to be 1137 GPa and 0.07, respectively. The values of Poisson's ratio used for silicon, fused silica, wood, and polypropylene were 0.28,[29] 0.17,[1] 0.45,[2] and 0.3, respectively.

C. Area measurement using AFM

A Quesant (Agoura Hills, CA) atomic force microscope (AFM) incorporated in the Triboindenter was used to image all residual indents. The AFM was operated in contact mode and calibrated using an Advanced Surface Microscopy Inc. (Indianapolis, IN) (www.asmicro.com)

calibration standard with a pitch of 292 ± 0.5 nm. Successive 4-μm scans and calibration routines revealed the reproducibility of the AFM calibration to be ±1%. Individual 4-μm field of view images were made of each indent and both z-height and lateral force images were analyzed as described below. ImageJ (http://rsb.info.nih.gov/ij/) image analysis software was used to manually measure the areas.

Figures 5(a)–5(c) show both z-height (right side) and lateral force (left side) images of indents in silicon, fused silica, and tracheid wall, respectively. Also included are surface profiles from the z-height images along the dashed lines in the figures (the profiles extend further than the images). The areas were measured by carefully identifying and manually outlining the edges of contact. For the silicon, which exhibits a small amount of pileup [Fig. 5(a)], the edge of contact was identified as the high point of the pileup. Indents in fused silica [Fig. 5(b)] and, to a lesser extent, in tracheid walls [Fig. 5(c)] exhibit sink-in behavior, and the edges of contact followed the resulting curvature. The method for determining the edge of contact primarily consisted of using the surface profiles to identify the edge of contact on the z-height image. In some cases, the lateral force images were also found to be useful and were used in tandem with the z-height images. For example, the corners of indents in fused silica [Fig. 5(b)] are more pronounced in the lateral force images than in the z-height images. Indents in the polypropylene (not shown) did not exhibit any noticeable pileup or sink-in behavior.

While undoubtedly the depth of the indent elastically recovers during unloading, one might question whether the contact edges of indents also recover after the indenter has been removed. However, Stillwell and Tabor[30] showed by direct experimentation on metals that there is an insignificant amount of elastic recovery in the diameter of the contact area for a conical indenter after unloading. Sakai and Nakano[31] also demonstrated for soda lime glass and poly(methyl methacrylate) (PMMA) that shrinkage of the projected area during unloading is negligible. The shrinkage in area during unloading is expected to be most notable in materials with high H/E_s ratios. Our materials have H/E_s ratios that are comparable to or lower than those of PMMA and soda lime glass. Therefore, we shall assume that the areas measured by identifying and outlining the contact edges from an AFM image obtained after the indenter has been removed are the same as those that existed at maximum load.

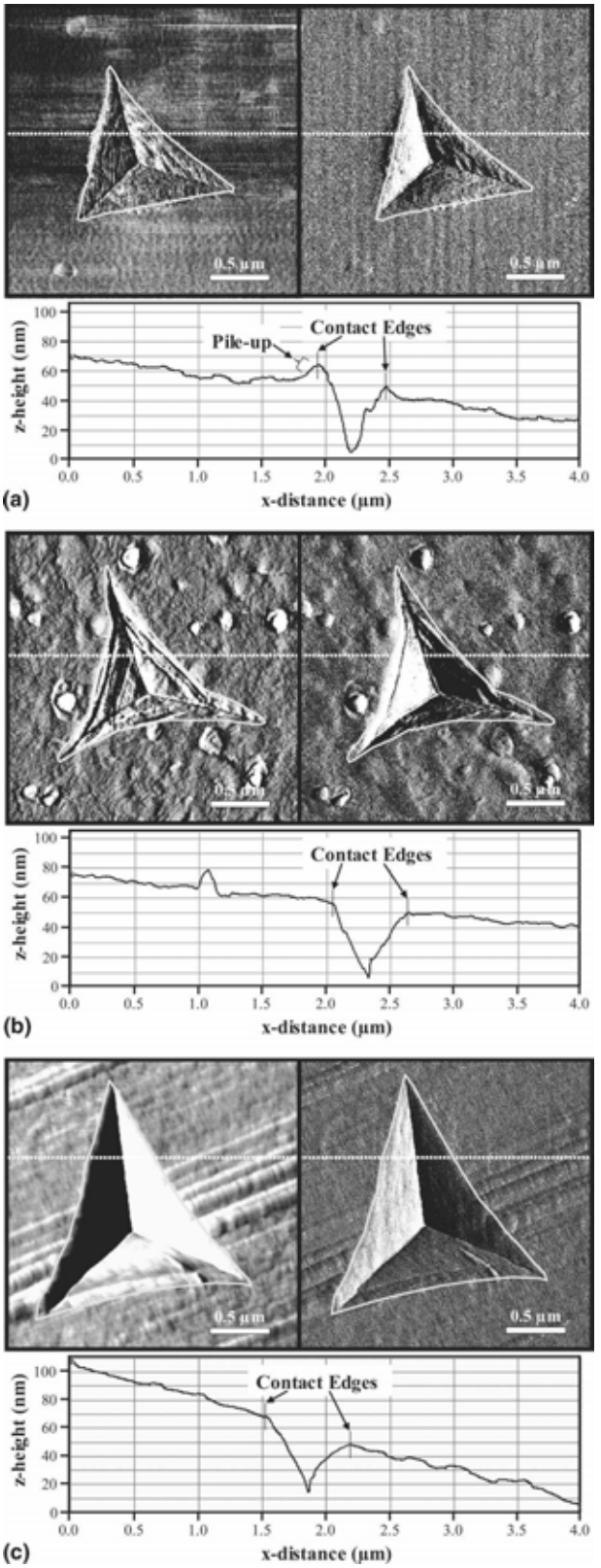

FIG. 5. Lateral force (left) and z-height (right) images of (a) 9.6 mN indent in silicon, (b) 9.6 mN indent in fused silica, and (c) 0.75 mN indent in S2 layer of a tracheid wall. The outlines of the measured contact areas are shown. The surface profile is taken from the dashed line in the z-height image but extends beyond the displayed image.

IV. EXPERIMENTAL RESULTS

A. Structural compliance in silicon bridge

To examine the effects of structural compliance on the measurement of E_s and H, a simple compliant bridge structure was constructed by attaching the ends of an

8 mm × 35 mm beam of silicon wafer to two 12-mm-diameter steel pucks with cyanoacrylate adhesive, as illustrated schematically in Fig. 6. Four series of indents, each consisting of five multiload indents (maximum loads of 2.0, 3.9, 5.8, 7.7, and 9.6 mN), were placed on the silicon bridge. One series (no. 1) was placed over the supported region, another was placed directly in the middle of the unsupported region (no. 4), and two additional series were placed between them (no. 2 and 3). It was anticipated that the structural compliance would be present only over the unsupported region and that it would increase as the distance from the supported region increased.

One way of accounting for the structural compliance is to construct a DN plot based on the measured areas. DN plots for the silicon bridge are shown in Fig. 7; they all have the same slopes but different intercepts, signifying that E_s remains constant and $C_m + C_s$ varies from one series to the next. As anticipated, $C_m + C_s$ increases with distance from the supported region. An alternative method for determining $C_m + C_s$ is to use SYS plots, as shown in Fig. 8. This correlation does not rely on the experimenter having to measure the areas of the indents. The 35 data points in each series come from the seven measurements for each of the five multiload indents in each series. The slopes of the curves are all different, corresponding to different $C_m + C_s$, but the intercepts are the same, suggesting the material properties (H/E_{eff}^2) are the same at each location. The average intercept is 0.604 ± 0.005 μm/N$^{1/2}$ (uncertainties reported are one standard deviation unless otherwise noted), an indication of the high level of precision that can be obtained from this method. The agreement in $C_m + C_s$ values obtained between the DN and SYS correlations is shown in Table II, where it can be observed that for series no. 1, the value of $C_m + C_s$ is very close to $C_m = 2.7 \pm 0.1$ μm/N, signifying the anticipated result that C_s is negligible over the rigidly supported region. Strictly speaking, according to Eq. (7), the individual curves in the SYS correlations are straight lines only if there is no indentation size effect in E_s and H. Close inspection of the curves in Fig. 8 reveals a tendency for $C_t L_{max}^{1/2}$ to deviate above the straight-line behavior at low loads, which is likely caused by an indentation size effect in $H^{1/2}/E_{eff}$. The indentation size effect appears to be rather weak and cannot be detected in the E_s and H values calculated over the range of loads used in this experiment [Figs. 9(a) and 9(b)]. Nevertheless, because of this weak indentation size effect in the data of Fig. 8, when we fitted the lines to the data we

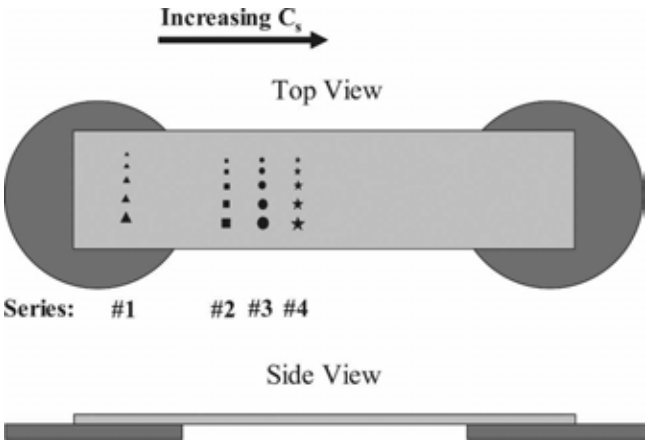

FIG. 6. Series of multiload indents performed on a silicon beam. The series numbers represent the corresponding data in Figs. 7–9 and Table II.

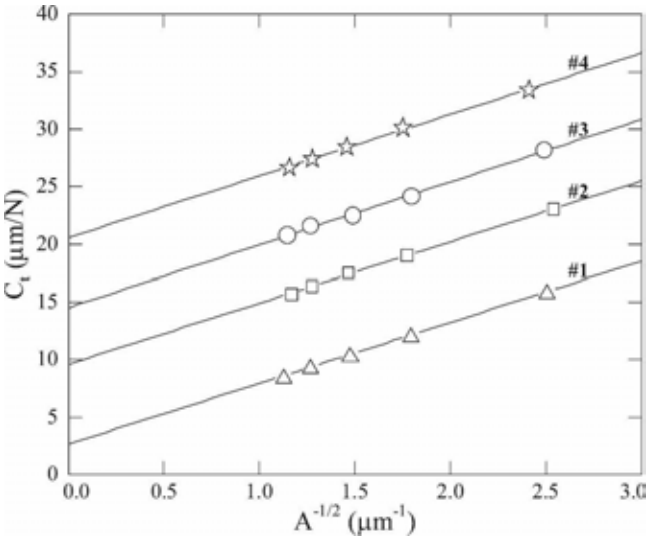

FIG. 7. DN plots for corresponding series on silicon beam (see Fig. 6). The curves all have the same slope, which signifies that E_s is the same for each series; different intercepts mean that $C_m + C_s$ changes from one series to the next.

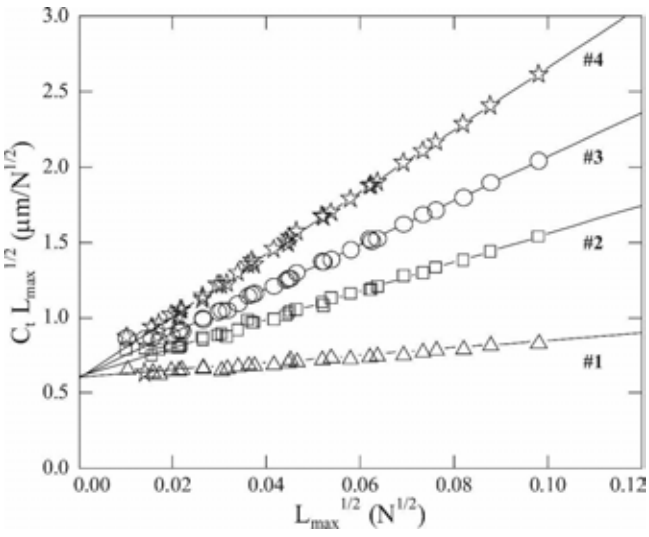

FIG. 8. SYS correlations for corresponding series on silicon beam (see Fig. 6). The curves all have the same intercept, which signifies that the material properties are the same for each series; different slopes mean that $C_m + C_s$ changes from one series to the next.

TABLE II. Data from a series of indents performed on silicon beam.[a]

Series	From SYS $J_0^{1/2}$ ($\mu m/N^{1/2}$)	From series H (GPa)	From DN E_s (GPa)	From SYS E_s (GPa)	From DN ($C_m + C_s$) ($\mu m/N$)	From SYS ($C_m + C_s$) ($\mu m/N$)
No. 1	0.606 ± 0.004	12.5 ± 0.2	165 ± 2	161 ± 3	2.7 ± 0.1	2.5 ± 0.2
No. 2	0.608 ± 0.007	12.7 ± 0.7	165 ± 3	161 ± 5	9.6 ± 0.2	9.5 ± 0.1
No. 3	0.606 ± 0.005	12.6 ± 0.5	161 ± 5	161 ± 3	14.5 ± 0.2	14.6 ± 0.1
No. 4	0.596 ± 0.006	12.3 ± 0.8	163 ± 5	162 ± 6	20.6 ± 0.2	20.6 ± 0.1

[a]All uncertainties are standard deviations except the data from the DN plots, which are based on a least squares analysis for corresponding linear fits.

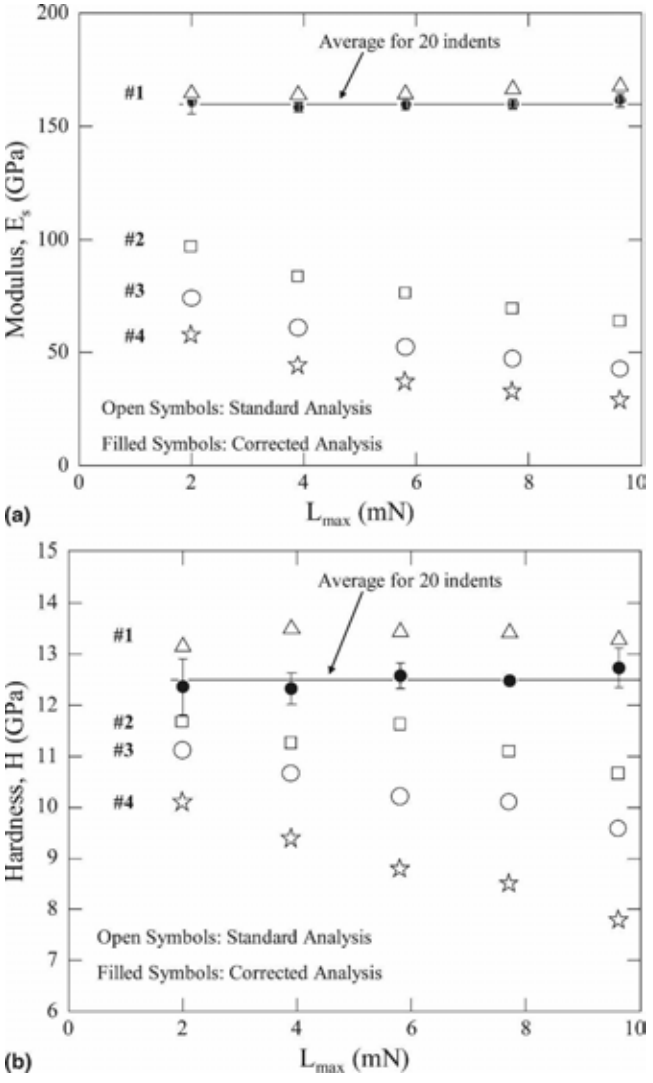

FIG. 9. Values of (a) E_s and (b) H calculated from the standard (open symbols) and corrected (solid symbols) analyses for the series of indents on the silicon beam. Each corrected value represents the average and standard deviation for the four indents performed at that load (one from each of the four series). The line represents the average value calculated from the corrected analysis for the 20 indents. Comparing the line to the values for the filled symbols reveals that no indentation size effect is present for the maximum loads used in this experiment.

excluded the data for $L_{max}^{1/2} < 0.025$ $N^{1/2}$. The fact that $C_m + C_s$ obtained from the SYS plot agrees with that obtained from the DN plot supports the assertion that the indentation size effect is weak.

To evaluate the necessity of taking into account C_s in the data analysis, we analyzed the data by calculating E_s and H directly from the raw data using the standard analysis [Eqs. (1)–(4)], which takes into account C_m but not C_s. Following the usual procedure for the standard analysis, we determined the areas of the indents from contact depth and the area function rather than relying on a direct measurement of area. In Figs. 9(a) and 9(b) these "standard analysis" data are compared with the corrected data, the latter of which rely not only on areas measured directly using AFM but also take into account both C_m and C_s obtained using the SYS plots. For the indents over the unsupported region (series no. 2–4), both E_s and H are underestimated by the standard analysis. One consequence of not accounting for C_s is that we overestimate C_p and therefore, from Eqs. (3) and (4), underestimate E_s. Moreover, by not taking into account C_s, we overestimate h_{max}. By virtue of Eq. (2), h_c depends on both C_s and h_{max}, and while the errors in C_s and h_{max} tend to partly cancel each other, the latter term dominates, a result of which is that h_c is overestimated. The area of the indent is therefore overestimated, which contributes to an underestimate of both E_s and H. It should be noted that if in the standard analysis C_s had been properly accounted for with the indents placed over the unsupported regions (series no. 2–4), the resulting E_s and H values would have agreed with the values obtained from the supported region (series no. 1).

We also compare our calculated values of E_s and H with the literature values. Using the standard Oliver–Pharr data analysis method, both Warren et al.[32] and Grillo et al.[33] indented (100)-oriented silicon and reported $E_s = 169$ GPa. For hardness, Warren et al. reported 12.2 GPa[32] and Grillo et al. reported 12.7 GPa.[33] With the standard analysis we calculate E_s and H values of 166 ± 2 and 13.4 ± 0.1 GPa, respectively, for the series of indents placed on the supported region of the silicon (series no. 1). Our measured value of hardness for silicon is higher than the values obtained by the other authors because the latter use $\beta = 1.128$ to calibrate the indenter shape, while we use $\beta = 1.23$.[24] Despite the difference in hardness values, our measured value of E_s agrees closely with the values in the literature because the effects of using different β values cancel out in the calculation of E_s when the standard analysis is used.

For the fully corrected analysis in which we measure the areas directly, we obtain 160 ± 3 GPa and 12.5 ± 0.3 GPa for E_s and H, respectively. These values are lower than the standard analysis values obtained calculated using calibrated areas and $\beta = 1.23$. However, the standard analysis suffers from the inability of the area function to account for the pileup formed near the indents in silicon [Fig. 5(a)]. We therefore believe the corrected values based on measured areas to be more accurate. Methods have been proposed to account for the pileup using an area function,[23] but measuring the areas directly from AFM images has the advantage of being able to account for pileup directly. Our corrected value of E_s also agrees well with the value of 159 GPa, which we obtain by taking into account crystal anisotropy based on the theory of Vlassak and Nix.[34] The value of 159 GPa was calculated using an anisotropy factor of 1.56[29] and a polycrystalline modulus of 165.6 GPa, which was based on the elastic constants of Hall.[35]

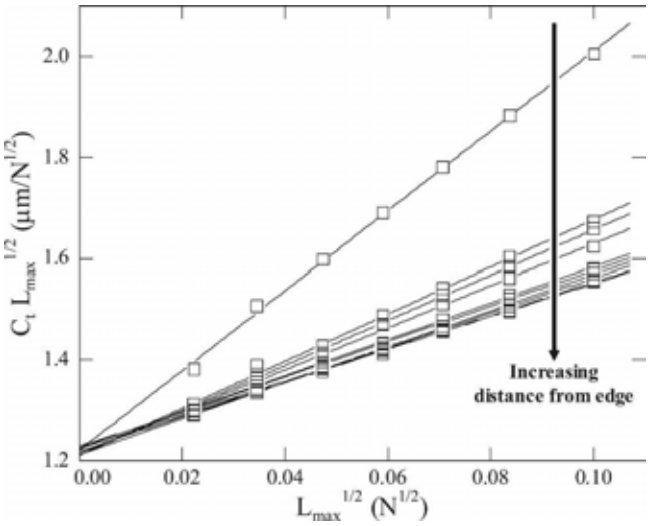

FIG. 11. SYS plots of multiload indents performed near edge of standard fused silica specimen. The slopes, and therefore $C_m + C_s$, decrease as the distance from the edge increases.

B. Edge effects in fused silica

To test the influence of a nearby free edge (drop-off) on the measurement of E_s and H, a fused silica standard was used as a specimen. A location was found along the perimeter of the specimen where the edge appeared both sharp and perpendicular, and at this location an array of multiload indents (maximum load 10 mN) was performed to obtain data at various distances from the edge. An AFM image of these indents is shown in Fig. 10. Some of the indents fell partly on the edge, and these we did not analyze. From the multiload indents, SYS plots were constructed (Fig. 11). To a very good approximation, almost all data from the different locations form straight lines and have the same intercept (1.218 ± 0.007 μm/N$^{1/2}$) but different slopes. The straight lines also suggest that the change in H due to changes in the plastic zone near the edge are negligible for the indents performed. Comparing Fig. 11 and the SYS plots from the compliant silicon bridge (Fig. 8), the inescapable conclusion is that the primary effect of an edge is to introduce a structural compliance.

The slopes in Fig. 11 show that as the distance from the center of the indent to the edge decreases, the slope, and therefore added structural compliance, increases. Using the corrected analysis, which accounts for this added structural compliance and uses areas measured directly from AFM images, we found that E_s and H remain constant as functions of distance from the edge (Fig. 12). We

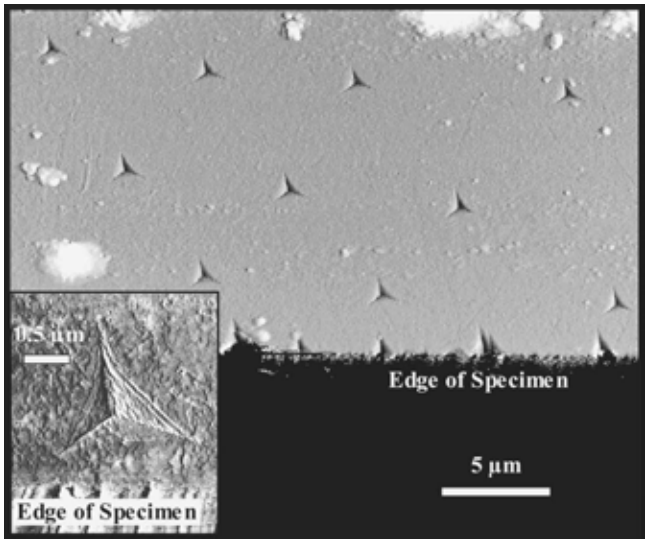

FIG. 10. AFM image of multiload indents performed near the edge of a fused silica specimen.

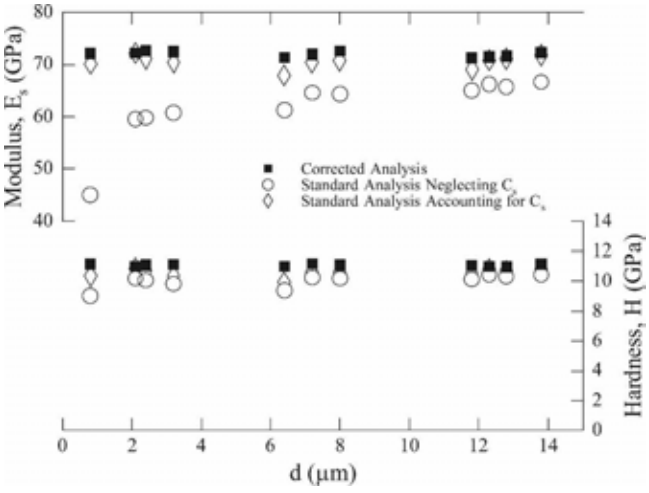

FIG. 12. Values of E_s and H calculated from the standard and corrected analyses of indents performed near the edge of a fused silica standard specimen. Distances from the edge (d) were measured from the center of the indents.

obtained 72.1 ± 0.5 GPa and 11.1 ± 0.1 GPa for E_s and H, respectively. For comparison, two sets of data based on the standard analysis are also displayed in Fig. 12. For one of these, C_s has been neglected, which results in both E_s and H appearing to decrease as the edge is approached. For the other set of data, we have accounted for C_s, which results in the values of E_s and H both being nearly independent of distance to the edge and agreeing with the values obtained based on the corrected analysis. The established literature value for E_s of fused silica is 72 GPa,[23] and our measurements of E_s do not differ substantially from this value, even when indents are placed to within 0.8 times their own diameters of the edge.

Dimensional analysis suggests that the added compliance caused by a nearby edge should be of the form

$$C_s = \frac{1}{Md} f\left(\frac{A^{1/2}}{d}\right) \quad . \tag{8}$$

where M is a relevant elastic modulus of the specimen, d is the distance from the center of the indent to the free edge, and f is some function depending on the size of the indent in relation to its distance to the edge. We anticipate that as $A^{1/2}/d \rightarrow 0$, then f approaches a constant because of Saint Venant's principle. To test the assertion of Eq. (8), we plotted the value of $C_m + C_s$ obtained from the SYS correlation against $1/d$ in Fig. 13. We find that the data form a straight line whose intercept is 3.0 ± 0.1 μm/N (uncertainty determined by least squares analysis of linear fit). This intercept represents the value of $C_m + C_s$ at an infinite distance from the edge, which for the fused silica standard should represent C_m, and indeed the intercept is close to our independent measurements of $C_m = 2.7 \pm 0.1$ μm/N. The data suggest that the function f is nearly constant even for large $A^{1/2}/d$.

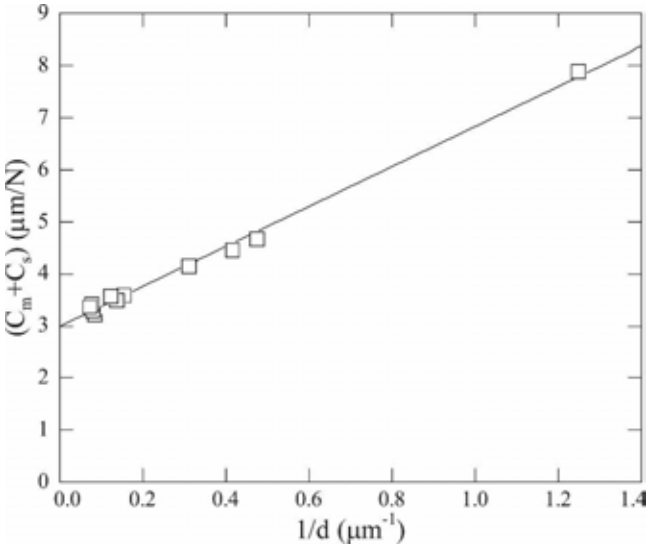

FIG. 13. Dependence of distance to edge on $C_m + C_s$ represented in the format of Eq. (8). Distances from the edge (d) were measured from the center of the indents.

C. Structural compliance effects in tracheid wall

In the first experiment on wood, a series of six multiload indents (maximum loads of 0.15, 0.30, 0.45, 0.60, 0.75, and 0.90 mN) were placed on a tracheid wall (Fig. 14) in an attempt to quantify C_s. The indents were all maintained at about the same distance from the edge of the tracheid wall so as to decrease the variation in compliance resulting from edge effects. The average value of $C_m + C_s$ obtained from the SYS plots was 7 ± 1 μm/N and agrees with $C_m + C_s = 8 \pm 2$ μm/N (uncertainty determined by least squares analysis of linear fit) obtained from the DN plot. The experimental data reveal that $C_m + C_s$ is higher than $C_m = 2.7$ μm/N by a factor of almost 3. We conclude, therefore, that the specimen possesses a substantial C_s. The corrected values of E_s and H are 19 ± 1 GPa and 510 ± 30 MPa, respectively, which are higher than the values of 16 ± 1 GPa and 450 ± 20 MPa that would have been obtained if the standard analysis had been used. The constant value of H calculated for this range of maximum loads also suggests that H is independent of load, which agrees with the assertion by Tze et al.[6] that wood lacks an indentation size effect.

To further investigate the variation of $C_m + C_s$ with proximity to the tracheid wall edge, a rectangular array of multiload indents (maximum load of 0.60 mN) was placed onto two, adjacent tracheid walls. Values of $C_m + C_s$ were calculated using SYS plots and the results are shown in Fig. 15. The ranges of $C_m + C_s$ in these figures are indicated using symbols located above the indents. Values of $C_m + C_s$ were calculated not only for indents that fell entirely within the tracheid walls but also for those that fell partially off the tracheid wall, having expanded during loading to extend into the lumen. For these latter indents, the low-load data in the multiload

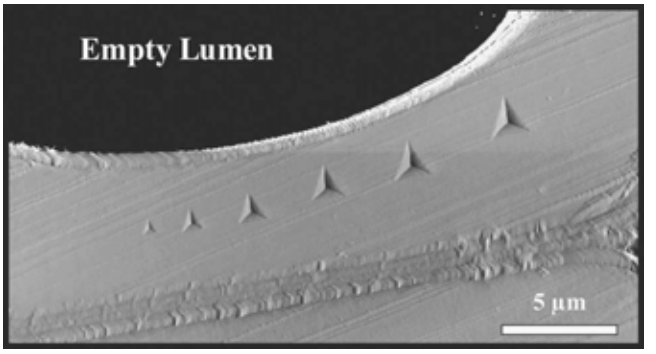

FIG. 14. AFM image of a series of multiload indents performed on a tracheid wall.

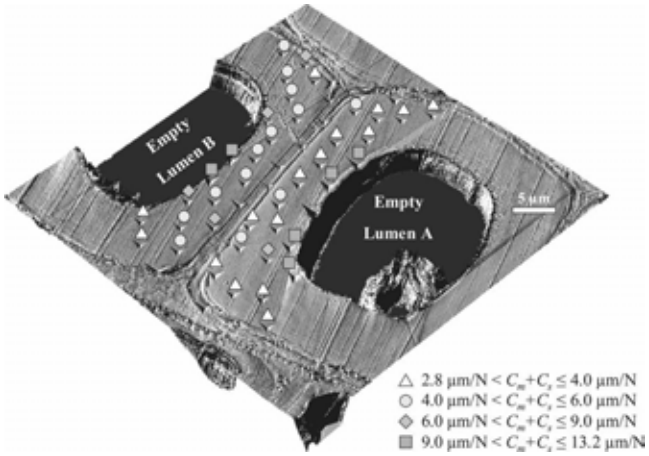

FIG. 15. Results from array of indents showing how $C_m + C_s$ depend on position across two, adjacent tracheid walls.

cycle [Fig. 4(b)] are still valid because at low loads the indent remains 100% in the wall. By excluding the data from the higher loads of the multiload indent from the fitting of the SYS correlation, we can remove the effects of the indents falling partially off the tracheid in the determination of $C_m + C_s$.

The values of $C_m + C_s$ in Fig. 15 range from 2.8 to 13.2 μm/N, with the indents closest to the empty lumen exhibiting higher values of $C_m + C_s$ consistent with the edge effects in fused silica described in the previous section. In principle, with the wood tracheids, the added structural compliance C_s can come from edge effects resulting from the proximity of the lumen and middle lamella or from the flexing of the tracheid wall. To help distinguish between these two contributions, a plot employing the concept of Eq. (8) was created using the $C_m + C_s$ data (Fig. 16). This plot is a first-order approximation because it assumes that only the distance from the center of the indent to the nearest lumen needs to be taken into account. A structural compliance arising from the flexing of the cellular structure would be expected to be relatively constant throughout the array of indents in Fig. 15. However, the intercept of Fig. 16 is 2.5 ± 0.4 μm/N (uncertainty determined by least squares analysis of linear fit), which corresponds closely to $C_m = 2.7 \pm 0.1$ μm/N. This result suggests the added structural compliance is primarily caused by the proximity of indents to the edge of the lumen rather than the flexing of the cellular structure.

Tze et al.[6] published nanoindentation data on loblolly pine specimens embedded in epoxy resin. They reported values calculated using the standard analysis in the ranges of 13.3 to 17.9 GPa and 340 to 460 MPa for E_s and H, respectively. These values are within the range of values calculated in this study, 19 ± 1 GPa and 510 ± 30 MPa for E_s and H, respectively, suggesting that the effects of the epoxy embedment are not strong. However, there are known to be large variations in properties of wood, even from the same species or within a single tree, depending on such factors as from which growth ring the specimen was taken and cardinal direction.[36] Therefore, a more direct comparison is necessary to determine if there is any effect from the epoxy embedment.

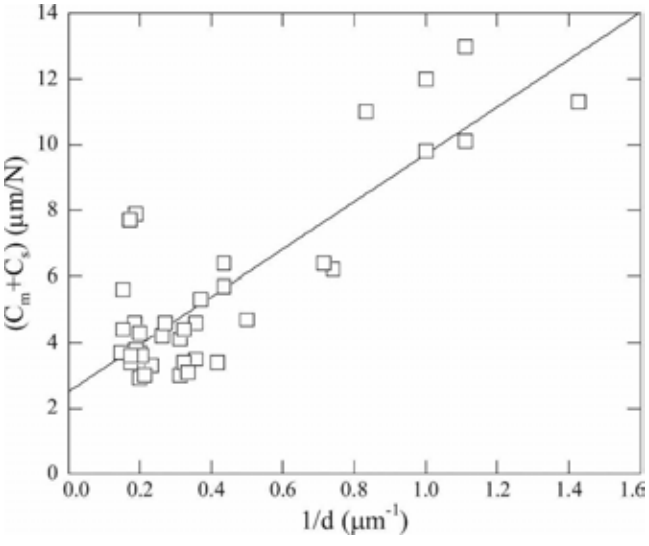

FIG. 16. Correlation between $C_m + C_s$ and distance (d) measured from the center of the indent to the nearest lumen.

D. Elastic discontinuities in wood–polypropylene composite

An AFM image of the composite is shown in Fig. 17. The roughness in the polypropylene matrix is believed to be chatter marks caused by the microtome procedure. A

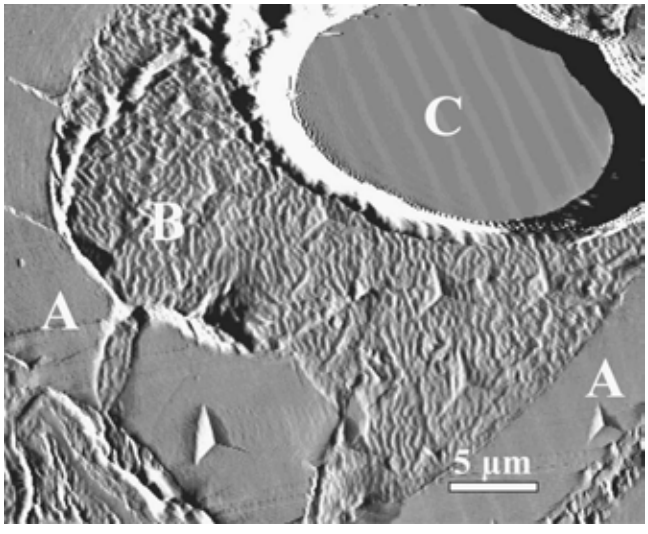

FIG. 17. AFM image of a mainly intact wood cell (A) with a lumen filled with polypropylene (B). Inside the polypropylene-filled lumen, a void (C) is also present. Indents placed in the polypropylene within the lumen were analyzed.

survey of the prepared surface with both a light microscope and AFM revealed that only a few wood tracheids remained intact within the composite. In the polypropylene matrix outside the lumens of the intact tracheids, there is a high density of small filler particles. Apparently, these filler particles are filtered out when the liquid polypropylene flows into the lumens of intact tracheids during manufacture. The filler pieces greatly increase the scatter in the measured properties,[37] and for this reason we report only the results of measurements performed in the polypropylene inside the lumen (Fig. 17), which lacks the filler particles.

Multiload indents were performed at various distances from the tracheid wall inside the filled lumen with maximum loads ranging from 0.3 to 1 mN. The SYS correlations for all of the multiload indents are displayed in Fig. 18. The values of $C_m + C_s$ obtained from the slopes range from −75 to 34 μm/N, with the negative slopes corresponding to indents that are close to the tracheid wall and the positive slopes corresponding to indents near cracks at debonded interfaces or voids in the polypropylene. The average intercept is $J_0^{1/2} = 3.6 \pm 0.1$ μm/N$^{1/2}$. Using the measured areas and data from the SYS correlations, the average calculated corrected values of E_s and H were 2.7 ± 0.2 GPa and 170 ± 30 MPa, respectively. As discussed in Jakes et al.,[37] these properties were found not to vary with distance to nearby structural heterogeneities, neither cell walls, voids, nor cracks, when the corrected analysis was used.

With the composite it is possible to correlate $C_m + C_s$ from a SYS plot with location in the specimen. We find that the best correlation is obtained if we take into account the presence of both the tracheid walls and the voids or cracks. In this case, we define an effective distance, d_{eff}, according to

$$\frac{1}{d_{eff}} = \frac{1}{d_h} - \frac{1}{d_w} \quad , \tag{9}$$

where d_h is the distance from the center of the indent to the nearest void or crack and d_w is the distance from the center of the indent to the nearest tracheid wall well-adhered to the polypropylene. Poorly adhered polypropylene–wood interfaces with obvious cracks were treated the same as holes. The correlation between $C_m + C_s$ and $1/d_{eff}$ is shown in Fig. 19. Again, the intercept of the fit, 3 ± 2 μm/N (uncertainty determined by least squares analysis of linear fit), corresponds well with $C_m = 2.7 \pm 0.1$ μm/N. The ability to establish this linear correlation based on two features of the structure suggests that it may be possible to estimate the effects of multiple elastic heterogeneities on C_s by merely adding their individual contributions. Of course, it is not necessary to predict beforehand the combined effects of multiple heterogeneities: the combined effects can be measured directly using the SYS correlation.

V. DISCUSSION

A. Theory for contact near an edge

For indentation against an infinite half-space, the elastic displacements die away in inverse proportion to the square of distance from the indent, which means that most of the elastic rebound comes from the material in the immediate vicinity of the indent. In this ideal limit, there is no additional structural compliance. However, specimens are never infinite in extent, and the finite size and shape of a real specimen will always give rise to

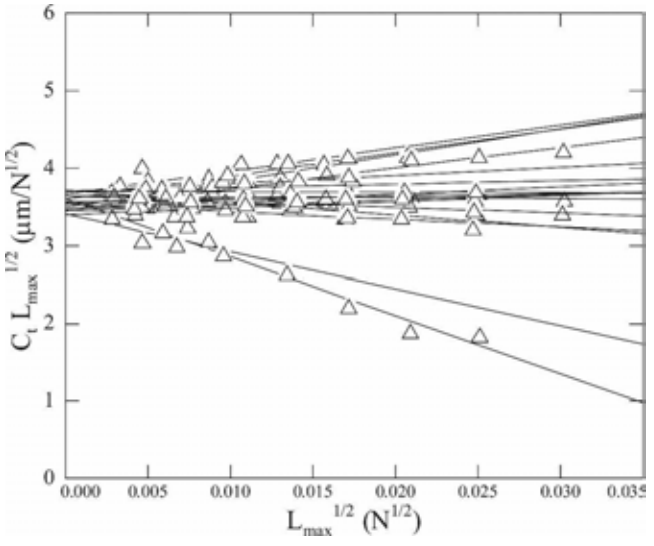

FIG. 18. SYS correlations for multiload indents performed in the polypropylene matrix of a polypropylene–wood composite within the lumen of an intact tracheid.

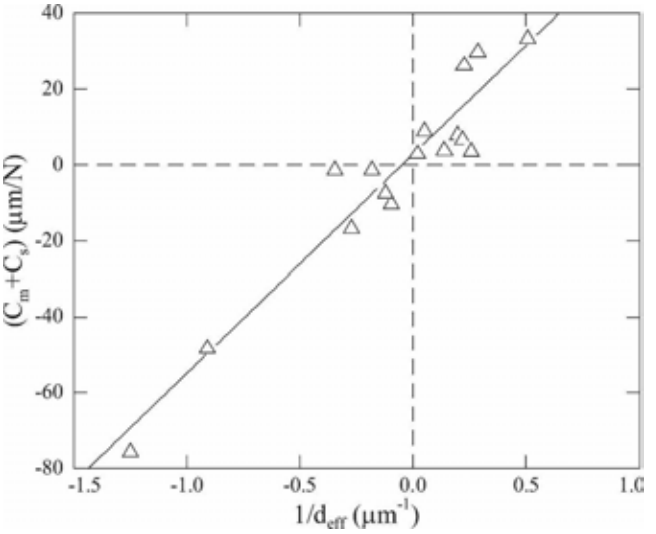

FIG. 19. Plot of $C_m + C_s$ as a function of $1/d_{eff}$ for indents placed in the polypropylene matrix of a polypropylene–wood composite.

displacements that originate from the long-range stress fields. These latter types of displacements are responsible for the first type of structural compliance that we have considered here [Fig. 2(a)]. In our experiments on silicon we established a situation where the flexing of the specimen under load gives rise to displacements that are large enough to appreciably affect the measurements. A well-supported cylindrical or prismatic specimen would be much more rigid, but it, too, would have a finite structural compliance, which can be estimated by the familiar formula h_s/E_0A_s, where h_s is the height of the specimen, E_0 is Young's modulus, and A_s is the cross-sectional area. For the wood specimens, with height 10 mm and cross-sectional area 100 mm^2, the estimated structural compliance is 0.01 μm/N based on a Young's modulus of 10 GPa for bulk wood. This value of C_s cannot be detected in our experiments. On the other hand, for more compliant specimens, nanoindentation can provide a sensitive method for probing this type of structural compliance as a function of position in the specimen.

The second type of structural compliance arises from elastic discontinuities at free edges and interfaces intersecting the surface [Fig. 2(b)]. Only a few studies have treated the problem of contact near an edge.[38–43] Notably, Hetenyi[39] found the solution for a point force acting on one surface of a quarter-space, the other surface of which is unconstrained. From Hetenyi's solution, Gerber[38] treated the problem of a frictionless, rigid, square indenter pushing against a quarter-space. More recently, Schwarzer et al.[43] investigated contact of a ball indenter near a free edge, and Popov[42] published a solution for Boussinesq contact in a quarter-space fully constrained on the lateral surface. Gerber shows that there is not only a force of contact but also a net moment. We have borrowed Gerber's results for the force part of the solution, taken from Gerber's Fig. 5.8,[38] and have replotted them by normalizing compliance and using $A^{1/2}/d$ as the abscissa in Fig. 20. Also included in Fig. 20 are the results of King's[12] analysis for a square, rigid indenter acting on the surface of a half-space, which represent the approach of the quarter-space problem in the limit $A^{1/2}/d \rightarrow 0$. The theoretical calculations in Fig. 20 verify that at least to a good approximation there is a linear relationship between structural compliance and $1/d$. The same figure shows that according to theory, C_s is approximately independent of $A^{1/2}$, which from our perspective is useful because that means that C_s is independent of size of the indent as suggested by our experiments. Empirically, the slopes of the curves vary in an approximately linear fashion on Poisson's ratio, so we can summarize the data in Fig. 20 with

$$C = \frac{(1-\nu^2)}{1.18E_{\text{eff}}A^{1/2}} + \frac{0.20 + 0.11\nu}{Ed} \quad , \qquad (10)$$

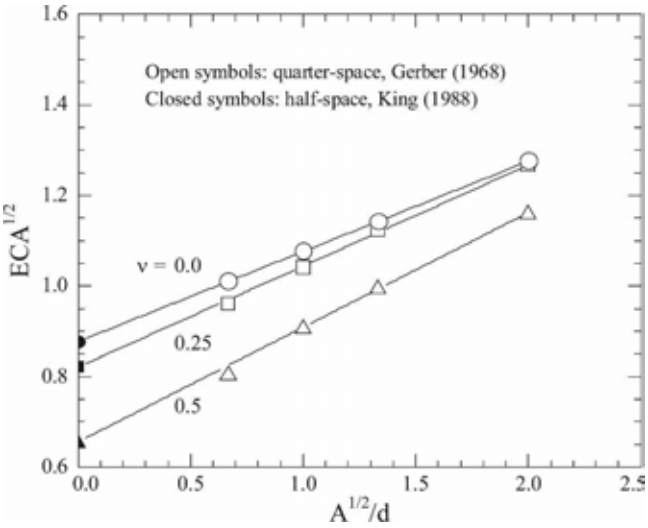

FIG. 20. Theory for effect of distance to free edge on measured compliance. E is Young's modulus, C is compliance, A is area, and d is distance from center of indent to free edge.

where the first term on the right-hand side takes into account the properties of both indenter and specimen and the numerical factor 1.18 is β as determined by King.[12] The second term on the right-hand side of Eq. (10) is C_s, the modification caused by the presence of an edge. For fused silica, the predicted value of the numerical factor that multiplies $1/d$ in Eq. (10) is 3.1 μm^2/N (E = 72 GPa, ν = 0.17), which is about 18% lower than the experimental value in Fig. 13 (slope = 3.8 μm^2/N). The agreement between theory and experiment is reasonable given that the simulation is for a square instead of a triangular indenter and that the actual distribution of stress might be skewed because of the combined effects of the moment introduced by the edge and the redistribution of stress caused by plastic deformation. Also, in our experiment the edge might not have been exactly the 90° assumed in Gerber's analysis.

There is a similarity between indentation of the edge geometry [Fig. 2(b)] and that of thin-film geometry [Fig. 2(c)]. In principle, it is not possible to treat the effect of the substrate in terms of a mere structural compliance, C_s, which is independent of the size of the indent. Instead, for the thin-film geometry, the effect of the substrate depends on how small the indent is made compared with the film thickness. However, simulations using the model of Stone[13] show that for small indents, with $A^{1/2}/d$ less than about 1 (here, d is film thickness), the constant compliance approximation becomes valid. Under these conditions the effect of the underlying substrate is to introduce a structural compliance which is nearly independent of the size of the indent. The sign of C_s depends on whether the substrate has a higher or lower modulus of elasticity than the film. For $A^{1/2}/d > 1$, the constant compliance approximation breaks down for the thin-film geometry.

B. Use of the DN and SYS plots as alternative methods for determining $C_m + C_s$

Both DN and SYS plots can be used to measure $C_m + C_s$, and each approach has its advantages and disadvantages. The DN plot is the more direct way to determine $C_m + C_s$. The method requires, however, that the areas of the indents be measured directly rather than determined based on contact depth, h_c, because knowledge of $C_m + C_s$ is required before h_c can be calculated. It also requires that C_s be uniform for all the indents, which is a disadvantage when C_s varies rapidly as a function of position. For the SYS plot, $C_m + C_s$ can in theory be determined without having to measure the areas of the indents because the correlation does not rely on direct knowledge of those areas. The SYS plot is also most easily used if there is no indentation size effect in the properties, in which case the plot is a straight line. It helps, therefore, to verify that there is no indentation size effect in, say, the hardness by directly measuring the areas of the indents and calculating the hardness from those measurements. Regardless of the method used to determine $C_m + C_s$, it is beneficial in the data analysis to measure the areas of the indents. However, even if there is an indentation size effect, one may identify whether the properties are changing from point to point by examining the intercept in the SYS plot, which does not require that the areas be measured.

VI. SUMMARY

An experimental procedure has been developed to account for structural compliances (C_s) in nanoindentation measurements. Similar to machine compliance (C_m), C_s is independent of load and contributes additively to the measured compliance. In this work, we investigated sources of C_s arising from (i) the large-scale flexing of the specimen and (ii) the presence of elastic heterogeneities, such as a nearby free edge and a stiff reinforcement phase that intersects the material perpendicular to the surface. Our methods account for C_s by employing and modifying correlations originally presented by Doerner and Nix[25] (DN plots) and Stone et al.[14] (SYS plots). In addition, contact areas of the indents are measured directly from AFM images. This allows E_s and H to be calculated with a minimum of error. Following are some of our important findings:

(1) DN and SYS plots can both measure C_s, but SYS plots can be used to measure C_s for individual indent locations. For these individual indent locations, the compliance is obtained as a function of load.

(2) The experimentally observed effect of a nearby elastic heterogeneity is to introduce a structural compliance C_s. Elastic theory supports this observation. To place an indent near a free edge results in a positive C_s. To place an indent near a stiffer phase results in a negative C_s. In both cases, the magnitude of C_s depends on the distance to the interface. To place an indent near both a free edge and stiffer phase results in a C_s whose magnitude depends on the proximity of both heterogeneities.

(3) The presence of C_s causes the standard Oliver–Pharr analysis to produce systematic errors in E_s and H if C_s is not taken into account. However, accounting for C_s prior to using the standard Oliver–Pharr analysis can remove those errors.

(4) The C_s present in nanoindentation experiments on tracheid walls is primarily an effect of the nearby free edge of the lumen, not the overall cellular structure of wood.

REFERENCES

1. W.C. Oliver and G.M. Pharr: Improved technique for determining hardness and elastic modulus using load and displacement sensing indentation experiments. *J. Mater. Res.* **7**(6), 1564 (1992).
2. R. Wimmer, B.N. Lucas, T.Y. Tsui, and W.C. Oliver: Longitudinal hardness and Young's modulus of spruce tracheid secondary walls using nanoindentation technique. *Wood Sci. Technol.* **31**(2), 131 (1997).
3. R. Wimmer and B.N. Lucas: Comparing mechanical properties of secondary wall and cell corner middle lamella in spruce wood. *IAWA J.* **18**(1), 77 (1997).
4. W. Gindl, H.S. Gupta, and C. Grunwald: Lignification of spruce tracheid secondary cell walls related to longitudinal hardness and modulus of elasticity using nano-indentation. *Can. J. Bot.* **80**(10), 1029 (2002).
5. W. Gindl, H.S. Gupta, T. Schoberl, H.C. Lichtenegger, and P. Fratzl: Mechanical properties of spruce wood cell walls by nanoindentation. *Appl. Phys. A: Mater.* **79**(8), 2069 (2004).
6. W.T.Y. Tze, S. Wang, T.G. Rials, G.M. Pharr, and S.S. Kelley: Nanoindentation of wood cell walls: continuous stiffness and hardness measurements. *Composites Part A: Appl. Sci.* **38**(3), 945 (2007).
7. W. Gindl and H.S. Gupta: Cell-wall hardness and Young's modulus of melamine-modified spruce wood by nano-indentation. *Composites Part A: Appl. Sci.* **33**(8), 1141 (2002).
8. W. Gindl, T. Schoberl, and G. Jeronimidis: The interphase in phenol-formaldehyde and polymeric methylene di-phenyl-di-isocyanate glue lines in wood. *Int. J. Adhes. Adhes.* **24**(4), 279 (2004).
9. J. Konnerth and W. Gindl: Mechanical characterisation of wood-adhesive interphase cell walls by nanoindentation. *Holzforschung* **60**(4), 429 (2006).
10. G.A. Zickler, T. Schoberl, and O. Paris: Mechanical properties of pyrolysed wood: a nanoindentation study. *Philos. Mag.* **86**(10), 1373 (2006).
11. G.E.L. Franco, D.S. Stone, and R.D. Blank (unpublished work, 2005).
12. R.B. King: Elastic analysis of some punch problems for a layered medium. *Int. J. Solids Struct.* **23**(12), 1657 (1987).
13. D.S. Stone: Elastic rebound between an indenter and a layered specimen. *I. Model.: J. Mater. Res.* **13**(11), 3207 (1998).
14. D.S. Stone, K.B. Yoder, and W.D. Sproul: Hardness and elastic modulus of TiN based on continuous indentation technique and new correlation. *J. Vac. Sci. Technol., A* **9**(4), 2543 (1991).
15. K.B. Yoder, D.S. Stone, R.A. Hoffman, and J.C. Lin: Elastic rebound between an indenter and a layered specimen. II. Using contact stiffness to help ensure reliability of nanoindentation measurements. *J. Mater. Res.* **13**(11), 3214 (1998).
16. Y. Choi, K.J. Van Vliet, L. Ju, and S. Suresh: Size effects on the

onset of plastic deformation during nanoindentation of thin films and patterned lines. *J. Appl. Phys.* **94**(9), 6050 (2003).
17. Y.M. Soifer, A. Verdyan, M. Kazakevich, and E. Rabkin: Edge effect during nanoindentation of thin copper films. *Mater. Lett.* **59**(11), 1434 (2005).
18. D. Ge, A.M. Minor, E.A. Stach, and J.W. Morris, Jr.: Size effects in the nanoindentation of silicon at ambient temperature. *Philos. Mag.* **86**(25), 4069 (2006).
19. A. Hodzic, Z.H. Stachurski, and J.K. Kim: Nano-indentation of polymer-glass interfaces. I. Experimental and mechanical analysis. *Polymer* **41**(18), 6895 (2000).
20. T.D. Downing, R. Kumar, W.M. Cross, L. Kjerengtroen, and J.J. Kellar: Determining the interphase thickness and properties in polymer matrix composites using phase imaging atomic force microscopy and nanoindentation. *J. Adhes. Sci. Technol.* **14**(14), 1801 (2000).
21. S-H. Lee, S. Wang, G.M. Pharr, and H. Xu: Evaluation of interphase properties in a cellulose fiber-reinforced polypropylene composite by nanoindentation and finite element analysis. *Composites Part A: Appl. Sci.* **38**(6), 1517 (2007).
22. A.C. Fischer-Cripps: Critical review of analysis and interpretation of nanoindentation test data. *Surf. Coat. Tech.* **200**(14), 4153 (2006).
23. W.C. Oliver and G.M. Pharr: Measurement of hardness and elastic modulus by instrumented indentation: Advances in understanding and refinements to methodology. *J. Mater. Res.* **19**(1), 3 (2004).
24. M. Troyon and S. Lafaye: About the importance of introducing a correction factor in the Sneddon relationship for nanoindentation measurements. *Philos. Mag.* **86**(33), 5299 (2006).
25. M.F. Doerner and W.D. Nix: A method for interpreting the data from depth-sensing indentation instruments. *J. Mater. Res.* **1**(4), 601 (1986).
26. D.L. Joslin and W.C. Oliver: New method for analyzing data from continuous depth-sensing microindentation tests. *J. Mater. Res.* **5**(1), 123 (1990).
27. W. Gindl and T. Schoberl: The significance of the elastic modulus of wood cell walls obtained from nanoindentation measurements. *Composites Part A: Appl. Sci.* **35**(11), 1345 (2004).
28. A.E. Slaughter: *Design and Fatigue of a Structural Wood–Plastic Composite* (Washington State University, Pullman, WA, 2004).
29. R. Hull: *Properties of Crystalline Silicon* (IEE, 1999), pp. xxvi+1016.
30. N.A. Stillwell and D. Tabor: Elastic recovery of conical indentations. *Proc. Phys. Soc.* **78**(2), 169–179 (1961).
31. M. Sakai and Y. Nakano: Elastoplastic load–depth hysteresis in pyramidal indentation. *J. Mater. Res.* **17**(8), 2161 (2002).
32. O.L. Warren, A. Dwivedi, T.J. Wyrobek, O.O. Famodu, and I. Takeuchi: Investigation of machine compliance uniformity for nanoindentation screening of wafer-supported libraries. *Rev. Sci. Instrum.* **76**(6), 62209 (2005).
33. S.E. Grillo, M. Ducarroir, M. Nadal, E. Tournie, and J.P. Fauriel: Nanoindentation of Si, GaP, GaAs and ZnSe single crystals. *J. Phys. D: Appl. Phys.* **36**(1), 5 (2003).
34. J.J. Vlassak and W.D. Nix: Measuring the elastic properties of anisotropic materials by means of indentation experiments. *J. Mech. Phys. Solids* **42**(8), 1223 (1994).
35. J.J. Hall: Electronic effects in the elastic constants of n-type silicon. *Phys. Rev.* **161**(3), 756 (1967).
36. S. Cramer, D. Kretschmann, R. Lakes, and T. Schmidt: Earlywood and latewood elastic properties in loblolly pine. *Holzforschung* **59**(5), 531 (2005).
37. J.E. Jakes, J.C. Hermanson, and D.S. Stone: Nanoindentation of the interphase region of a wood-reinforced polypropylene composite, in *Proceedings of the Ninth International Conference on Woodfiber-Plastic Composites*, (Madison WI, 21–23 May, 2007), pp. 197–203.
38. C.E. Gerber: Contact Problems for the Elastic Quarter-Plane and for the Quarter Space (Stanford University, Palo Alto, CA, 1968), p. 100.
39. M. Hetenyi: Method of solution for elastic quarter-plane. *Trans. ASME Series E, J. Appl. Mech.* **27**(2), 289 (1960).
40. M. Hetenyi: A general solution for the elastic quarter space. *Trans. ASME Series E, J. Appl. Mech.* **37**(1), 70 (1970).
41. L.M. Keer, J.C. Lee, and T. Mura: Contact problem for the elastic quarter space. *Int. J. Solids Struct.* **20**(5), 513 (1984).
42. G.Y. Popov: An exact solution of the mixed elasticity problem in a quarter-space. *Mech. Solids* **38**(6), 23 (2003).
43. N. Schwarzer, I. Hermann, T. Chudoba, and F. Richter: *Contact Modelling in the Vicinity of an Edge* (Elsevier, San Diego, CA, 2001), pp. 371–377.